Available online at www.sciencedirect.com
ScienceDirect
C. R. Mecanique 335 (2007) 280–286
COMPTES RENDUS MECANIQUE
http://france.elsevier.com/direct/CRAS2B/

Melting and solidification: processes and models/Flows in solidification

A thermo-hydraulic numerical model to study spot laser welding

Marc Medale [a,*], Charline Xhaard [a,b], Rémy Fabbro [c]

[a] *Polytech'Marseille et IUSTI, UMR 6595 CNRS-université de Provence, technopole de Château-Gombert, 5, rue Enrico-Fermi, 13453 Marseille cedex 13, France*
[b] *CEA Valduc, DFTN/SPAC/LSO, 21000 Is-sur-Tille, France*
[c] *CLFA/LALP, UPR CNRS 1578, 16 bis, avenue Prieur de la Côte d'Or, 94114 Arcueil cedex, France*

Abstract

The aim of this study is to better understand the basic mechanisms leading to defect occurrence in spot laser welding. For that purpose we have developed a numerical model, which takes into account the key-hole dynamics together with a dedicated energy deposition model featuring the multiple reflection effects. Many experiments have also been achieved enabling us to report several defect classes. The analysis of some of these scenarios have been performed, and favourably compared to experiments. ***To cite this article: M. Medale et al., C. R. Mecanique 335 (2007).***

Résumé

Un modèle numérique thermo-hydraulique pour l'étude du soudage laser impulsionnel. L'objectif de cette étude vise à mieux comprendre les mécanismes de base à l'origine de défauts en cours de soudage par laser impulsionnel. Dans ce but, nous avons développé un modèle numérique qui tient compte de la dynamique de creusement en mode key-hole, ainsi qu'un modèle de dépôt d'énergie incluant les effets de réflexions multiples. Plusieurs expériences ont permis de mettre en évidence divers types de défauts. Les simulations numériques de certains de ces scénarios ont été effectuées et comparées aux résultats éxpérimentaux. ***Pour citer cet article : M. Medale et al., C. R. Mecanique 335 (2007).***

Keywords: Computational fluid mechanics; Spot laser welding; Free and moving interface

Mots-clés : Mécanique des fluides numérique ; Soudage laser impulsionnel ; Surface libre et mobile

Version française abrégée

Le procédé de soudage par laser impulsionnel permet d'assembler des pièces métalliques par une succession d'impacts, produisant chacun une fusion très localisée de la matière constituant le joint. De ce fait, ce procédé limite au minimum l'étendue de la zone affectée thermiquement et par conséquent l'effet des modifications micro-structurales à l'origine des contraintes et déformations résiduelles. Cependant, pour assurer la fiabilité des liaisons soudées il est capital de maîtriser le comportement de la zone de soudage. En effet, la sévérité des cycles thermiques subis peut

* Corresponding author.
E-mail address: Marc.Medale@polytech.univ-mrs.fr (M. Medale).

1631-0721/$ – see front matter
doi:10.1016/j.crme.2007.05.013

néanmoins entraîner des contraintes et déformations à l'échelle des structures. De plus, les mouvements du métal liquide au sein du métal fondu (bain de soudage) sont à l'origine de nombreux défauts, tels que porosités et cavités, qui peuvent altérer rédhibitoirement l'intégrité des soudures.

L'objectif de cette étude consiste donc à caractériser l'évolution thermo-hydraulique d'un impact laser réalisé sur une plaque en TA6V (alliage composé de titane, d'aluminium et de vanadium). L'identification des phénomènes physiques a permis de distinguer les différentes étapes de l'interaction entre le faisceau laser et la matière. Sous l'effet de l'intensité lumineuse, le métal fond, puis se vaporise. La détente de la vapeur engendre une pression sur le film liquide à l'origine de la déformation de la surface du bain liquide, faisant ainsi apparaître une cavité appelée capillaire de soudage. En conséquence, le métal liquide expulsé par cet « effet piston » à l'interface liquide–gaz vient s'accumuler en périphérie de ce cratère près de la surface. Le capillaire de soudage piège le faisceau laser, ce qui a pour principal effet d'augmenter le taux de puissance absorbée par la matière (absorptivité équivalente). À la fin de l'impact laser, sous l'effet combiné de la gravité et surtout des forces de tension superficielle, le métal liquide accumulé en surface retombe dans le capillaire où il se solidifie.

Le modèle numérique est basé sur une approche à maillage mobile permettant d'appréhender la déformation de l'interface liquide–gaz, sans introduire de distorsion rédibitoire du maillage dans le domaine de calcul (approche ALE, [12]). Pour le cas d'un impact isolé considéré dans cette étude, le problème présente une symétrie de révolution. Les évolutions thermiques et hydrodynamiques sont déterminées à partir de la résolution des équations de conservation de la masse, de la quantité de mouvement et de l'énergie dans les phases condensées (solide et liquide). Les changements de phase solide–liquide et liquide–vapeur sont pris en compte par une approche enthalpique. La phase gazeuse est considérée comme une condition aux limites du problème d'hydraulique : la pression induite par le phénomène de vaporisation est modélisée par une adaptation de la loi de Clausius–Clapeyron aux cinétiques rapides. Le flux thermique issu de l'interaction entre le faisceau laser et la matière est obtenu par le calcul du trajet optique des photons, basé sur les lois de Fresnel, pour prendre en compte le piégeage du faisceau laser dans le capillaire. La validation du modèle numérique s'appuie sur la confrontation avec les résultats expérimentaux obtenus. Les résultats numériques permettent d'appréhender la dynamique du creusement du trou capillaire, ainsi que les éventuels scénarios d'apparition de porosité lors de l'effondrement du capillaire en fin d'interaction laser.

1. Introduction

Compared with other welding processes, spot laser welding offers several advantages in industrial manufacturing. Indeed, localized temperature gradients require weaker global heating, so one could consequently expect lower workpiece distortions. Therefore spot laser welding processes are well suited to problems in which the allowed Affected Heat Zone is required to remain as small as possible in the vicinity of the welded joins. Unfortunately, the operating parameters leading to defect-free welded joins are difficult to obtain, owing to a relatively poor understanding of the problem. Consequently, unsafe welded joins are repeatedly encountered, polluted by micro or macro pore defects.

In order to better understand why and how these defects occur, both experimental and numerical approaches have been undertaken [1,2]. From the computational point of view, at least three major types of difficulties have to be overcome to design robust and accurate numerical models well suited to the spot-laser-welding class of problems:

(i) The laser-beam energy deposition onto a moving and highly deforming interface (keyhole) requires dedicated numerical models, even if the gas phase is not ionized (no plasma). Indeed, the laser beam is trapped in the keyhole and undergoes multiple reflections along the liquid–gas interface. Several models based on Fresnel's laws have been developed to account for the local energy concentration over the lower part of the keyhole [3,4];
(ii) The multiphase problem (solid–liquid–gas) is not straightforward to deal with, especially for alloys made up of several metals. A few authors have proposed to solve the incompressible Navier–Stokes equations in all phases (solid, liquid and gas) [5,6]. Nonetheless, the relevance of such models becomes questionable in the gas phase, where the Mach number could reach values up to 0.5;
(iii) The algebraic system resulting from the discretization of this class of problems is very stiff (ill-conditioned) from the numerical point of view, owing to the strong material and geometrical coupling. It remains up-to-now computationally expensive to solve. For these reasons analytical and semi-analytical approaches are still widely used in the keyhole dynamics models [7–9], as far as three-dimensional effects could not be neglected [10].

2. Physical and numerical models

The present model has been designed to study the dynamics of a single-laser-pulse over a thin metal plate. The axial-symmetry condition is assumed in both; no ionization of the metallic vapours and shield gas throughout the whole transient study, together with no beam diffusion inside the vapours. Furthermore, the coupled fluid flow and heat transfer model is focused on the condensed phases (solid and liquid), whereas the dispersed phases (metallic vapours and shield gas) have been modelled in the simplest way, so that they enter the model as boundary conditions of the former model.

The numerical model is built in the finite element framework and takes advantage of the segregated approach [11,12]. Indeed, it consists in splitting the whole problem into subproblems, easier to build up and also to solve successively. The four stages considered in our model are the following: (i) compute the laser-beam energy deposition; (ii) compute the heat transfer in the whole computational domain; (iii) compute the fluid flow in the liquid phase, if any; (iv) perform a computational domain update to satisfy the mass conservation in the condensed phase. The resulting solution algorithm consists in consecutively solving these four stages at each time step of the whole transient.

2.1. Laser-beam energy deposition model

Let us first consider at this stage that the geometry of the computational domain is entirely defined at a given time, as are its boundaries. Consequently, one can discretize the laser-beam into concentric annuli, and based on Fresnel's laws, for each ray-tube leaving the beam, one can determines its whole optical path throughout multiple reflections, if any, along the keyhole. The intensity of the ray-tubes prior to their first incidence is modeled by a Gaussian expression [13]:

$$I(r,z) = \frac{2P}{\pi\omega^2(z)}\exp\left(\frac{2r^2}{\omega^2(z)}\right), \quad \omega(z) = \omega_0\sqrt{1+\left(\frac{z}{z_R}\right)^2} \tag{1}$$

Along the optical path, at each ray interaction with the condensed matter, a part of the incident optical power is transmitted, whereas the remainder is reflected with an angle equal to the angle of incidence with respect to the outward normal (Fresnel's laws). Indeed, for rather low power density Nd:Yag laser applications, as in the present case, the metallic vapours remain so poorly ionised that one can assume they are perfectly transparent to laser rays, the unlike the case for CO_2 lasers. Therefore, the transmitted power density only depends on both the incidence angle and the local temperature at the incident location. The absorbed intensity along the liquid–gas interface corresponds to the sum of the energy density transmitted to the condensed matter at each local interaction. It acts in our numerical model as an applied heat flux given by the expression:

$$q_{\mathrm{lb}}(\beta,T) = \sum_{\text{ray annulii}}\left(\sum_{\text{reflections}} I(r,z)\alpha(\beta,T)\right) \tag{2}$$

This heat flux represents the boundary source term in the heat transfer model.

2.2. Heat transfer model

The macroscopic model dedicated to the condensed phases is derived from the two-phase model [14,15]. Therefore, the conservation equations of mass, momentum and energy apply on the whole condensed matter domain with physical properties specific to each phase. In the present case, the applied flux density induces solid–liquid and liquid–vapour phase changes. The enthalpy formulation of the energy conservation equation is used:

$$\frac{{}^*\rho_i(c_{p_i}T+\Delta h)}{{}^*t} + (\mathbf{u}-\mathbf{w})\cdot\nabla\left[\rho_i(c_{p_i}T+\Delta h)\right] - \nabla\cdot(k_i\nabla T) = 0 \tag{3}$$

where the subscript designates either solid, mushy or liquid phase, respectively. As the computational domain has moving and deforming boundaries, the conservation equations are written in an arbitrary-Lagrangian–Eulerian formulation.

The thermal boundary conditions can be split into four parts. The first is associated with the axial-symmetry condition (adiabatic condition along the symmetry axis); the second is the applied heat flux associated with the laser

beam interaction (q_{lb}); the third boundary condition models the rate of thermal energy devoted to vaporization or condensation, if any. It is accounted for in our model as a boundary condition over the liquid–vapour interface, as follows:

$$q_{\mathrm{lv}} = m_{\mathrm{lv}} \Delta h_{\mathrm{lv}}; \quad \rho_{\mathrm{l}} \mathbf{v}_{\mathrm{l}/\Sigma} \cdot \mathbf{n} = \rho_{\mathrm{v}} \mathbf{v}_{\mathrm{v}/\Sigma} \cdot \mathbf{n} \tag{4}$$

The vaporization rate is drawn from the mass balance across the liquid–vapour interface. Finally, the fourth thermal boundary condition is associated with the radiative and convective heat transfer over the other boundaries of the condensed phase domain. They are modelled in a simple way as:

$$q_{\mathrm{rc}} = \sigma \varepsilon \left(T^4 - T_\infty^4\right) + h(T - T_\infty) \tag{5}$$

2.3. *Fluid flow model*

The heat transfer in the condensed phases is significantly dominated by advection in the melted pool, where the liquid metal flow is modelled as an incompressible fluid flow. Nevertheless, the basic Navier–Stokes equations should be slightly modified to account for the inter-dendrites fluid flow at the macroscopic scale [16]. Therefore, the mass and momentum conservation equations read:

$$\nabla \cdot \mathbf{u} = 0; \quad \rho_{\mathrm{l}} \left[\frac{\partial \mathbf{u}}{\partial t} + (\mathbf{u} - \mathbf{w}) \cdot \nabla \mathbf{u} \right] = \nabla \cdot \bar{\bar{\sigma}} + \mathbf{f}^v + \mathbf{S}^u \tag{6}$$

The first constitutive law used to close the preceding set of equations is that of a Newtonian fluid. Secondly, the Boussinesq approximation is used to take into account buoyancy in the incompressible fluid flow model. Finally, a source term has been selectively introduced in the mushy zone to model at the macroscopic scale the fluid flow which takes place at microscopic scale close to solid–liquid interface, according to a Darcy-like flow in a porous media.

The boundary conditions (see Fig. 1) that apply to the liquid metal fluid flow problem read in a formal notation:

$$\mathbf{u} = \mathbf{0} \quad \text{on } \partial\Omega_{\mathrm{sl}}; \qquad \mathbf{T} = \bar{\bar{\sigma}} \cdot \mathbf{n} = \mathbf{T}^{\partial\Omega} \quad \text{on } \partial\Omega_{\mathrm{lg}} \tag{7a,b}$$

The most important interactions between the gas phase and the liquid phase can be attributed to: (i) the recoil pressure associated with the evaporation process; (ii) the shear stress induced by the high velocity difference between dispersed phase and the liquid metal flow in the key hole; (iii) surface tension effects (capillary forces owing to

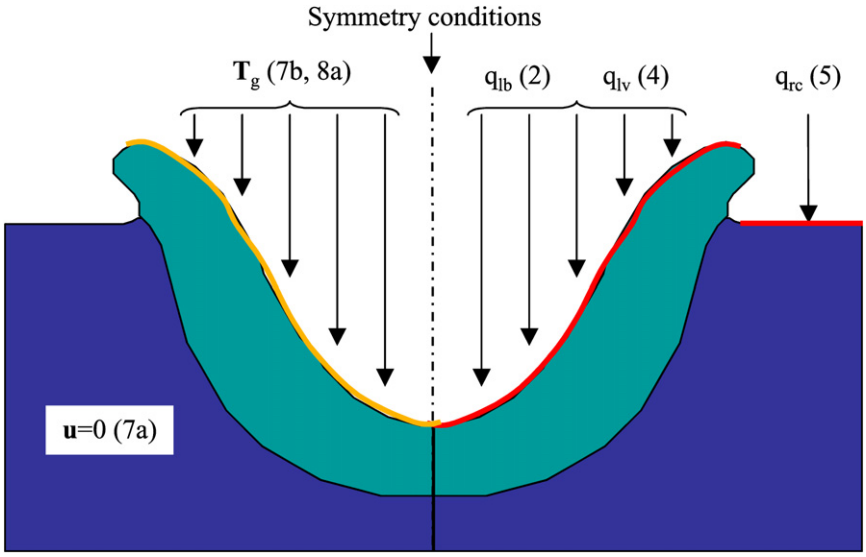

Fig. 1. Sketch of the applied boundary conditions for the computation: velocity field (left) and thermal field (right).

Fig. 1. Schéma des conditions aux limites appliquées : champs de vitesse (gauche) et de température (droite).

pressure difference across the interface, and thermo-capillary forces over the interface induced by surface tension gradients):

$$\mathbf{T}_\mathrm{l} + \mathbf{T}_\mathrm{g} + \frac{\gamma}{R}\mathbf{n} + \frac{\partial \gamma}{\partial s}\mathbf{t}_\mathrm{g} = 0 \quad \text{with } \gamma = \gamma_0 + \frac{\mathrm{d}\gamma}{\mathrm{d}T}(T - T_0) \tag{8a,b}$$

2.4. Computational domain update—Mesh adaptation model

As the computational domain is restricted to the condensed matter (solid and liquid phases), it evolves and deforms in the course of time. So, to prevent mesh distortion being responsible for poor solution accuracy, we supplement our numerical model with the solution at each time step of a steady pseudo-elastic problem for the mesh [12]. It is formulated in nodal mesh displacement variables in order to explicitly satisfy a kinematic boundary condition all over the fluid flow domain boundary. This kinematic condition states a vanishing normal component of the relative velocity between the liquid fluid flow and the mesh along the boundaries.

3. Analysis

We consider a single laser pulse carried out in the middle of a thin metal sheet (no junction zone), to satisfy the axial-symmetry condition. The delivered laser beam power is considered constant ($P = 1500$ W) throughout the 10 ms laser pulse. It is carried by an optical fiber and its spatial distribution over the metal sheet is assumed to be a 600 μm diameter top hat at the focal point. To later on compare the computations to experiments carried out in our CEA laboratory, TA6V alloy has been considered in the computation (physical properties provided in Table 1).

The finite element model has been first validated in simplified configurations [12,13]. So, the present study aims to validate the energy deposition model on a dynamically deforming keyhole where multiple reflections take place. As the free surface deforms to a large extent (keyhole) during the laser pulse, the laser energy deposition becomes of first concern, especially when multiple reflections occur in the keyhole. The physical domain is 3 mm thick (metal sheet thickness), and 1 mm wide, initially made up of TA6V alloy, at ambient room temperature $T_0 = 300$ K. In the computations, we assume constant physical properties (given in Table 1) all over the solid–liquid domain, and the simplified thermal heat exchange boundary conditions (5) are set to: $\varepsilon = 0.5$, $h = 10\ \mathrm{W\,m^{-1}\,K^{-1}}$ and $T_\infty = 300$ K. The mesh used in the present computations is made up of 75×150 bi-quadratic quadrilateral finite elements (Q9), non-uniformly distributed in the radial and axial directions, respectively. A constant time increment of 10^{-2} ms has been used, so the computation of the whole laser pulse requires 1000 time steps.

The recoil pressure applied onto the free surface induces a fast drilling of the keyhole. The computations faithfully reproduce this behaviour, as shown in Figs. 2 and 3 for $t = 2$ ms and $t = 7.5$ ms, respectively. As the keyhole becomes deeper and deeper the number of laser-rays reflections increases significantly, as can be observed in Fig. 3, which depicts a close up of the reflected ray paths in the vicinity of the keyhole tip, together with the corresponding thermal field, at time $t = 7.5$ ms. The multiple reflections inside the highly deformed keyhole result in a noticeable power intensity focus over the keyhole tip. Indeed the global absorptivity coefficient, which measures the energy efficiency

Table 1
Physical properties used for the TA6V alloy at 1923 K

Tableau 1
Propriétés physiques de l'alliage TA6V utilisé (à 1923 K)

Melting temperature (K)	1923
Vaporization temperature (K)	3591
Liquid density ($\mathrm{kg\,m^{-3}}$)	4110
Specific heat ($\mathrm{J\,kg^{-1}\,K^{-1}}$)	743
Thermal conductivity ($\mathrm{W\,m^{-1}\,K^{-1}}$)	35
Surface tension coefficient ($\mathrm{N\,m^{-1}}$)	1.6
Thermal coefficient of surface tension ($\mathrm{N\,m^{-1}\,K^{-1}}$)	3×10^{-4}
Viscosity (Pa s)	34×10^{-4}
Liquid–gas latent enthalpy ($\mathrm{J\,kg^{-1}}$)	8.8×10^{6}
Solid–liquid latent enthalpy ($\mathrm{J\,kg^{-1}}$)	0.4×10^{6}

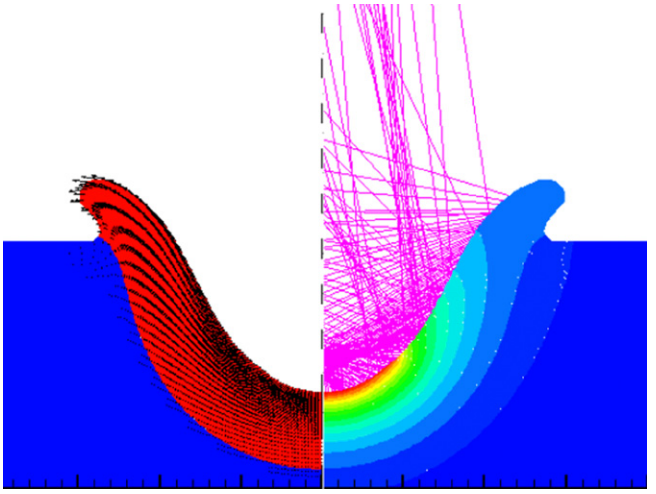

Fig. 2. Velocity field in the liquid metal (left), reflected rays at the liquid–gas interface and thermal field (right) at $t = 2$ ms.

Fig. 2. Champ de vitesses dans le métal liquide (gauche), rayons-laser réfléchis par la surface et champ de température (droite), à $t = 2$ ms.

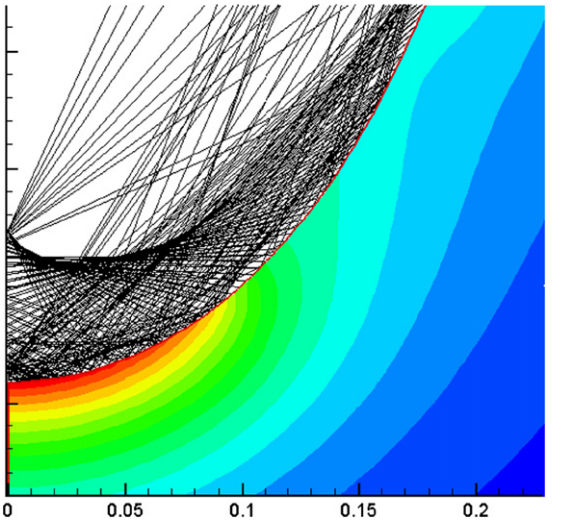

Fig. 3. Close-up of the tip of the key-hole: reflected rays at the liquid–gas interface and thermal field at $t = 7.5$ ms.

Fig. 3. Zoom de l'extrémité du capillaire de soudage : rayons-laser réfléchis par la surface du liquide et champ de température, à $t = 7{,}5$ ms.

of the interaction, raises from roughly 50% at the beginning of the laser pulse up to 80% as soon as the keyhole is deep enough to trap most of the reflected rays. The finite element mesh adaptation technique performs well to deal with the moving boundary problem in such a highly deformed computational domain, resulting in a fairly good accuracy over the whole computations.

4. Conclusions

This article presents the numerical model we have developed to study the dynamics of a single laser pulse acting on a thin metal sheet. This model problem is expected to provide us with a better understanding of the basic mechanisms that could be responsible for numerous defects in industrial spot laser welding processes. The numerical model is focused on the condensed phases (solid and liquid), but take into account the dispersed phase (vapours and shield gas) in a simplified manner. It is made up of four main stages: the laser energy deposition, the heat transfer in computational domain, the fluid flow in the liquid phase, if any, and finally a computational domain and mesh update to account for the total mass conservation and large distortion of the liquid–gas interface (keyhole). The present study deals with an intermediate level validation whose objective was the test and verification of the energy deposition model on a dynamically deforming keyhole where multiple reflections take place. As the free surface shape evolves continually during the laser pulse, the ray paths (determined by Fresnel's law) become of first concern to accurately compute the laser energy deposition, especially when multiple reflections occur in the keyhole.

References

[1] K. Girard, J.M. Jouvard, J. Boquillon, P. Bouilly, P. Naudy, Proc. SPIE Conf. (Bellingham, SPIE) 3888 (2000) 418–428.
[2] A. Kaplan, M. Mizutani, S. Katayama, A. Matsunawa, Unbounded keyhole collapse and bubble formation during pulsed laser interaction with liquid zinc, J. Phys. D: Appl. Phys. 35 (2002) 1218–1228.
[3] R. Fabbro, K. Chouf, Keyhole modelling during laser welding, J. Phys. D: Appl. Phys. 87 (2000) 4075–4083.
[4] E. Amara, A. Bendib, Modelling of vapour flow in deep penetration laser welding, J. Phys. D: Appl. Phys. 35 (2002) 272–280.
[5] R.K. Ganesh, A. Faghri, Y. Hahn, A generalized thermal modelling for laser drilling process—I. Mathematical modelling and numerical methodology, J. Heat Mass Transfer 40 (1997) 3351–3360.
[6] R.K. Ganesh, A. Faghri, Y. Hahn, A generalized thermal modelling for laser drilling process—II. Numerical simulation and results, J. Heat Mass Transfer 40 (1997) 3361–3373.
[7] W. Semak, W.D. Bragg, B. Damkroger, S. Kempkas, Temporal evolution of the temperature field in the beam interaction zone during laser-material processing, J. Phys. D: Appl. Phys. 32 (1999) 1819–1825.

[8] P. Solana, P. Kapadia, J.M. Dowden, P.J. Marsden, An analytical model for laser drilling of metals with absorption within the vapour, J. Phys. D: Appl. Phys. 32 (1999) 942–952.
[9] W.W. Duley, Laser Welding, Wiley Interscience, New York, 1999.
[10] J.M. Jouvard, K. Girard, O. Perret, Keyhole formation and power deposition in ND:YAG laser spot welding, J. Phys. D: Appl. Phys. 34 (2001) 2894–2901.
[11] H. Ki, P.S. Mohanty, H. Mazumder, Modelling of high density laser material interaction using fast level set method, J. Phys. D: Appl. Phys. 34 (2001) 364–372.
[12] S. Rabier, M. Medale, Computation of free surface flows with a projection FEM in a moving mesh framework, Comput. Methods Appl. Mech. Engrg. 192 (2003) 4703–4721.
[13] M. Medale, S. Rabier, C. Xhaard, A thermo-hydraulic numerical model for high energy welding processes, Rev. Eur. Elements Finis 13 (2004) 207–229.
[14] W.D. Bennon, F.P. Incropera, A continuum model for momentum, heat and species transport in binary solid–liquid phase change systems—1. Model formulation, 2. Application to solidification in a rectangular cavity, Int. J. Heat Mass Transfer 30 (1987) 2161–2187.
[15] J. Ni, F.P. Incropera, Extension of the continuum model for transport phenomena occurring during metal alloy solidification—1. The conservation equations, 2. Microscopic considerations, Int. J. Heat Mass Transfer 38 (1995) 1271–1296.
[16] V.R. Voller, C. Prakash, A fixed grid numerical modelling methodology for convection diffusion mushy region phase change problems, Int. J. Heat Mass Transfer 24 (1987) 1709–1718.